

Bayesian Convolutional Neural Networks for Compressed Sensing Restoration

Xinjie Lan, *Student Member, IEEE*, Xin Guo, *Student Member, IEEE*, Kenneth E. Barner, *Fellow, IEEE*,

Abstract—Deep Neural Networks (DNNs) have aroused great attention in Compressed Sensing (CS) restoration. However, the working mechanism of DNNs is not explainable, thereby it is unclear that how to design an optimal DNNs for CS restoration. In this paper, we propose a novel statistical framework to explain DNNs, which proves that the hidden layers of DNNs are equivalent to Gibbs distributions and interprets DNNs as a Bayesian hierarchical model. The framework provides a Bayesian perspective to explain the working mechanism of DNNs, namely some hidden layers learn a prior distribution and other layers learn a likelihood distribution. Moreover, the framework provides insights into DNNs and reveals two inherent limitations of DNNs for CS restoration. In contrast to most previous works designing an end-to-end DNNs for CS restoration, we propose a novel DNNs to model a prior distribution only, which can circumvent the limitations of DNNs. Given the prior distribution generated from the DNNs, we design a Bayesian inference algorithm to realize CS restoration in the framework of Bayesian Compressed Sensing. Finally, extensive simulations validate the proposed theory of DNNs and demonstrate that the proposed algorithm outperforms the state-of-the-art CS restoration methods.

Index Terms—Bayesian Compressed Sensing, Deep Neural Networks, Bayesian hierarchical model, Gibbs distribution.

I. INTRODUCTION

SAMPLING theory is a cornerstone of signal processing, which indicates that a band-limited signal can be precisely recovered from its uniform samples as long as the sampling rate is at least twice the bandwidth of this signal, namely the Nyquist rate [1]. However, the exponential growth of the Nyquist rate makes signal processing extremely difficult and complicated in the big data era. In other words, conventional sampling theory plagues our ability to acquire, transmit, and process high dimensional dataset, thereby spurring tremendous interest in novel sampling theories and techniques.

Compressive Sensing (CS) provides an alternative paradigm for sampling theory [2], [3]. In general, a K -sparse signal $\mathbf{x} \in \mathbf{R}^N$ is to be sampled by a linear measurement matrix $\mathbf{A} \in \mathbf{R}^{M \times N}$ ($M < N$), and the measurement \mathbf{y} can be written in matrix form as $\mathbf{y} = \mathbf{A}\mathbf{x} + \mathbf{n}$, where $\mathbf{n} \in \mathbf{R}^M$ is commonly assumed as Gaussian noise with variance σ_n^2 . If \mathbf{A} satisfies *Restricted Isometry Property* (RIP), CS guarantees that \mathbf{x} can be accurately restored from $M = \mathcal{O}(K \log(N/K))$ measurements with high probability [4], [5].

Among all traditional methods of CS restoration, Bayesian Compressed Sensing (BCS) has received much attention, since it can easily take into account the prior knowledge of \mathbf{x} , namely the inherent signal structures of \mathbf{x} , to improve CS restoration by specifying a prior distribution [6], [7], [8]. In the context of BCS, CS restoration is reformulated as a Bayesian posterior inference problem, in which the signal structure is expressed by a prior distribution $p(\mathbf{x}; \boldsymbol{\theta})$ and the likelihood distribution of CS is commonly formulated as a Gaussian distribution [9], [10]. After deriving the posterior distribution of CS given the prior and likelihood distributions, we can realize CS restoration by inferring the posterior distribution.

Since $p(\mathbf{x}; \boldsymbol{\theta})$ plays an important role in describing the signal structure of interest, the key of BCS is to choose a $p(\mathbf{x}; \boldsymbol{\theta})$ for modeling the signal structure precisely and comprehensively. Lots of prior distributions have been used to model various signal structures in the framework of BCS, e.g., Laplace distribution [9], Markov Random Fields (MRFs) [11], [12], [13], Spike and Slab model [14], [15], Gaussian Mixture Model (GMM) [16], [17], [18], [19]. However, the above prior distributions have two limitations. First, they commonly exploit hand-crafted linear filters, which are difficult to express the signal structure precisely unless taking lots of trials to modify the parameters of the filters. Second, they merely model the signal structure in a small neighborhood in order to reduce the complexity of parameter optimization, but most signal structures have abundant high-order dependencies [20]. As a result, they are difficult to describe the signal structure comprehensively as well.

As the resurgence of Deep Neural Networks (DNNs) in various applications like speech recognition [21] and image classification [22], DNNs have aroused considerable attention in CS restoration. Compared to traditional BCS algorithms, DNNs can precisely describe multiple signal structures based on their powerful representation ability [23] and efficient training algorithms [24]. More specifically, some works attempt to design an end-to-end DNNs to directly restore \mathbf{x} from \mathbf{y} for CS restoration [25], [26], [27]. Meanwhile, other works combine traditional CS restoration and DNNs to realize CS restoration [28], [29]. It is noteworthy that some DNNs present better performance than traditional BCS methods [26], [29].

However, a fundamental problem of DNNs is that they are vulnerable to perturbation [30], [31], [32], which results in bad CS restoration in noisy situation. Moreover, all existing theories cannot convincingly clarify the internal logic of deep learning and DNNs have been viewed as "black boxes" [33]. That means we still don't know how to design an optimal neural networks for CS restoration.

This material is based upon work supported by the National Science Foundation under Grant No. 1319598. The material in this paper was presented in part at IEEE GlobalSIP, Montreal, Canada, November 2017.

Xinjie Lan, Xin Guo, and Kenneth E. Barner are with Department of Electrical and Computer Engineering, University of Delaware, Newark, DE, 19711 USA (email: lxjbit, guoxin, barner@udel.edu)

In this paper, we attempt to shed light on the above problems and propose a novel algorithm for CS restoration based on DNNs. Overall, our contributions to this literature are three folds. First, we propose a novel statistical framework to explain the architecture of DNNs, which proves that the hidden layers of DNNs are equivalent to Gibbs distributions and interprets DNNs as a Bayesian hierarchical model. In particular, the proposed framework provides a novel Bayesian perspective to explain DNNs, namely some hidden layers are used to learn a prior distribution $p(\mathbf{X})$ and the remaining layers are responsible for learning a likelihood distribution $p(\hat{\mathbf{Y}}|\mathbf{X})$, where \mathbf{X} and $\hat{\mathbf{Y}}$ denote the random variables of the input and output of DNNs, respectively.

Second, we provide insights into DNNs in four aspects: (i) the application scope of DNNs is confine to the situation that the training dataset provides great or equal to the information of the training labels; (ii) we cannot achieve the state-of-the-art performance by simply applying DNNs to CS restoration. (iii) the activation function of DNNs cannot denoise very well, which is an important reason for the vulnerability of DNNs. (iv) we unify traditional BCS methods and DNNs and provide an overall picture of all BCS algorithms;

Third, we propose a novel CS restoration algorithm based on DNNs. In contrast to design an end-to-end DNNs for CS restoration, we propose a novel Convolutional Neural Networks (CNNs) to model a prior distribution $p(\mathbf{x}; \boldsymbol{\theta})$ only. In particular, the proposed CNNs have a dual property: (i) it has a closed-form expression as traditional prior distributions; (ii) it preserves the same powerful representation ability as DNNs. The duality enable the proposed CNNs to overcome the limitations of BCS and DNNs simultaneously. Given the prior distribution $p(\mathbf{x}; \boldsymbol{\theta})$ corresponding to the CNNs and the likelihood distribution of CS, we derive the posterior distribution of CS and propose a novel Bayesian inference algorithm to realize CS restoration.

This paper is organized as follows. Section II lays out the necessary background related to this topic. We describe the proposed statistical framework to explain DNNs in Section III. Subsequently, Section IV proposes the insights into DNNs. Section V presents the proposed CS restoration algorithm. In the end, numerical simulations validate our proposed theory and algorithm in Section VI.

II. BACKGROUND

This section reviews three fundamental topics related to our research: Gibbs distribution, BCS, and DNNs.

A. Gibbs Distribution

In statistical mechanics, a Gibbs distribution is a probability measure that gives the probability of a certain state as a function of the state's energy and system temperature, which can be expressed as

$$p_k(\mathbf{x}; \boldsymbol{\theta}) = \frac{1}{Z(\boldsymbol{\theta})} \exp[-\frac{1}{T} g_k(\mathbf{x}; \boldsymbol{\theta}_k)] \quad (1)$$

where \mathbf{x} indicate all samples in a system, $g_k(\mathbf{x}; \boldsymbol{\theta}_k)$ is the *energy function* of state k , and T is system temperature [34]. In addition, $Z(\boldsymbol{\theta}) = \sum_{k=1}^K \exp(-g_k(\mathbf{x}; \boldsymbol{\theta})/T)$ is the partition

function, K denotes the number of all states in the system of interest, and $\boldsymbol{\theta} = \bigcup_k \boldsymbol{\theta}_k$ indicate all parameters.

It is important to note that Gibbs distribution is equivalent to Markov Random Fields (MRFs), which can be formulated below [35], [36].

$$p(\mathbf{x}; \boldsymbol{\theta}) = \frac{1}{Z(\boldsymbol{\theta})} \exp[-\frac{1}{T} g(\mathbf{x}; \boldsymbol{\theta})] \quad (2)$$

In terms of MRFs, the *energy function* $g(\mathbf{x}; \boldsymbol{\theta})$ is defined as

$$g(\mathbf{x}; \boldsymbol{\theta}) = \sum_k f_k^{NL}(f_k(\mathbf{x}; \boldsymbol{\theta}_k)) \quad (3)$$

where $f_k^{NL}(f_k(\cdot))$ represents a clique potential function, and f_k^{NL} is a non-linear function, $f_k(\cdot)$ is a linear filter to describe local dependence [36]. The partition function $Z(\boldsymbol{\theta})$ is defined as $\sum_{\mathbf{x}} \exp(-g(\mathbf{x}; \boldsymbol{\theta})/T)$ in the context of MRFs.

Gibbs distribution, especially MRFs, is a commonly used prior distribution in BCS field, since it can easily derive an arbitrary distribution to model the signal structure of interest by redefining $g(\mathbf{x}; \boldsymbol{\theta})$ [11], [12], [13], [14]. Meanwhile, Gibbs distribution has various connections with DNNs [37], [38]. First, it has been proven that softmax layer is identical to Gibbs distribution [39], [40]. Second, some works demonstrate that a convolutional layer with an non-linear layer can be formulated as MRFs model [41], [42].

B. Bayesian Compressed Sensing

Given the expression of CS, namely $\mathbf{y} = \mathbf{A}\mathbf{x} + \mathbf{n}$, BCS converts CS restoration into a Bayesian posterior inference problem [8], [9], [10]. Since the noise \mathbf{n} is commonly assumed as a Gaussian distribution with unknown variance σ_n^2 , the likelihood distribution of CS can be formulated below.

$$p(\mathbf{y}|\mathbf{x}, \mathbf{A}, \sigma_n^2) = \frac{1}{\sqrt{(2\pi\sigma_n^2)^N}} \exp(-\frac{1}{2\sigma_n^2} \cdot \|\mathbf{A}\mathbf{x} - \mathbf{y}\|_2^2) \quad (4)$$

Assuming the prior distribution is expressed as a Gibbs distribution $p(\mathbf{x}; \boldsymbol{\theta})$ to describe the signal structure of interest, the posterior distribution $p(\mathbf{x}|\mathbf{A}, \mathbf{y}, \sigma_n^2)$ for CS restoration can be derived as follows given the above prior and likelihood distributions based on Bayes' theorem.

$$p(\mathbf{x}|\mathbf{A}, \mathbf{y}, \sigma_n^2) \propto p(\mathbf{y}|\mathbf{x}, \mathbf{A}, \sigma_n^2) \cdot p(\mathbf{x}; \boldsymbol{\theta}) \quad (5)$$

Moreover, the solution to CS restoration can be derived below based on the Maximum a Posteriori (MAP) principle.

$$\hat{\mathbf{x}}_{\text{BCS}} = \arg \min_{\mathbf{x} \in \mathbb{R}^N} \|\mathbf{A}\mathbf{x} - \mathbf{y}\|_2^2 + \frac{2\sigma_n^2}{T} \cdot g(\mathbf{x}; \boldsymbol{\theta}) \quad (6)$$

The above equation suggests that $\hat{\mathbf{x}}_{\text{BCS}}$ crucially depends on $g(\mathbf{x}; \boldsymbol{\theta})$, which describes the signal structure of interest. However, an unsolved problem of $g(\mathbf{x}; \boldsymbol{\theta})$ is to derive optimal linear filters $f_k(\cdot)$ for modeling the signal structure precisely and comprehensively. Initially, hand-crafted linear filter $f_k(\cdot)$ is directly utilized to model signal structure [14], [15], which needs lots of trials to obtain good CS restoration. Expectation-Maximization (EM) method is commonly explored to optimize $f_k(\cdot)$, but it still cannot model the signal structure precisely since it requires too many hyper-parameters [17]. Meanwhile, existing methods only describe signal structure in a small neighborhood, but most signal structures have abundant high-order dependencies [20], which means that $f_k(\cdot)$ is hard to simulate the signal structure comprehensively.

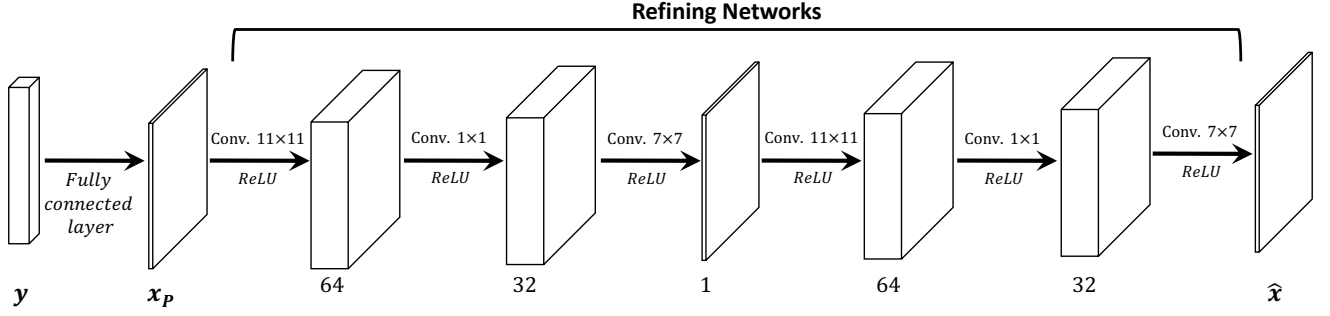


Fig. 1: The architecture of DNNs for CS restoration. This figure also illustrate an existing DNNs for CS restoration, namely ReconNet [25], which uses a single fully connected layer to obtain x_P and six convolutional layers (abbr. Conv.) to refine x_P . The third block represents a convolutional layer of ReconNet consist of 64 linear filters with dimension 11×11 .

C. Deep Neural Networks for CS restoration

Because of their powerful representation ability [23] and efficient training algorithms [24], DNNs have the potential to solve the aforementioned problem of BCS. Consequently, numerous efforts recently have been devoted to applying DNNs to CS restoration field [28], [25], [26], [27], [29].

Since standard DNNs can be viewed as a function projecting the high dimensional input, such as an image dataset, to the low dimensional output like classification labels, the most intuitive way of designing DNNs for CS restoration is to reverse standard DNNs as Fig. 1. More specifically, the DNNs first use fully connected layers to derive a preliminary restoration x_P , and take advantage of the powerful representation ability of convolutional layers to refine x_P for deriving the final restoration \hat{x} . In particular, the sub-networks for refining x_P is called refining networks here.

Initially, previous works like ReconNet [25] directly apply the DNNs to CS restoration. Nevertheless, they only exhibit similar restoration as BCS algorithm, and even worse than the later in some cases. Subsequently, DR2Net remodels the refining networks as residual networks, namely $\hat{x} = x_P + x_R$, and achieves better CS restoration than ReconNet [26], [43]. Meanwhile, some works combine traditional CS restoration and DNNs [28], [29]. For instance, Learning Denoiser Approximate Message Passing (LDAMP) uses a traditional CS restoration method, i.e., Approximate Message Passing (AMP)

[17], [18], to obtain x_P , and utilizes the refining networks to derive x_P . In other words, LDAMP regards the refining networks as a powerful denoiser and integrates it into the traditional AMP method. It is noteworthy that LDAMP and DR2Net achieve better CS restoration than traditional BCS. Fig. 2 shows the architecture of the three networks.

Though some DNNs like LDAMP outperforms traditional BCS algorithms, a problem of DNNs for CS restoration is that DNNs are vulnerable to perturbation [30], [31], [32]. This problem implies that DNNs cannot precisely reconstruct input x from noisy measurement y [26]. More importantly, another fundamental problem of DNNs is that the working mechanism of DNNs is still not explainable and DNNs have been viewed as "black boxes" [33]. Therefore, we still don't have an explicit theory to explain how design an optimal DNNs for a specific application like CS restoration.

III. A STATISTICAL FRAMEWORK OF DNNs

This section describes the proposed statistical framework of DNNs. We demonstrate that the hidden layers of DNNs are equivalent to Gibbs distributions and the whole architecture of DNNs can be interpreted as a Bayesian hierarchical model.

To facilitate subsequent discussions, we assume that an arbitrary neural networks with I hidden layers denoted as $\{\mathbf{X}; \mathbf{F}_1; \dots; \mathbf{F}_I; \hat{\mathbf{Y}}\}$ is trained by \mathcal{X} and \mathcal{Y} , where $\mathcal{X} = \{\mathbf{x}_n | \mathbf{x}_n \in \mathbf{R}^{W \times H}, n = 1, \dots, N\}$ denotes a training dataset and $\mathcal{Y} = \{\mathbf{y}_n | \mathbf{y}_n \in \{0, 1\}^{L \times 1}, n = 1, \dots, N\}$ are training labels. \mathbf{X} and \mathbf{Y} are the random variables related to \mathcal{X} and \mathcal{Y} , respectively. Similarly, \mathbf{F}_i and $\hat{\mathbf{Y}}$ are the random variables for the i th hidden layer and output layer.

A. A Statistical Representation of Hidden Layers

Proposition 1: The hidden layers of a neural network are equivalent to Gibbs distributions of the network input.

Suppose there is a shallow neural network $\{\mathbf{X}; \mathbf{F}; \hat{\mathbf{Y}}\}$, in which \mathbf{F} has K neurons and $\hat{\mathbf{Y}}$ is softmax layer (Figure 3), each output node $\hat{y}_l \in \hat{\mathbf{y}} = \{\hat{y}_1, \dots, \hat{y}_L\}$ therefore can be formulated as

$$\hat{y}_l = \frac{1}{Z} \exp\left\{\sum_{k=1}^K \beta_{lk} \cdot f_k^{act}[f_k(\mathbf{x})]\right\} \quad (7)$$

where $\mathbf{x} \in \mathcal{X}$ is the input, $f_k^{act}(\cdot)$ is the activation function of the k th neuron, $f_k(\mathbf{x}) = (\sum_{m=1}^{M=W \times H} \alpha_{km} \cdot x_m)$, and α_{km} ,

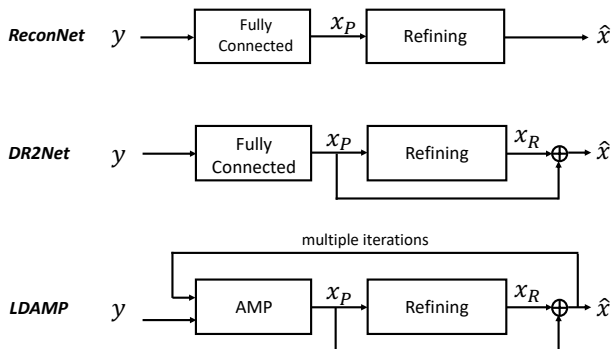


Fig. 2: The architectures of three neural networks for CS restoration, y denotes a CS measurement, and \hat{x} is the restored signal.

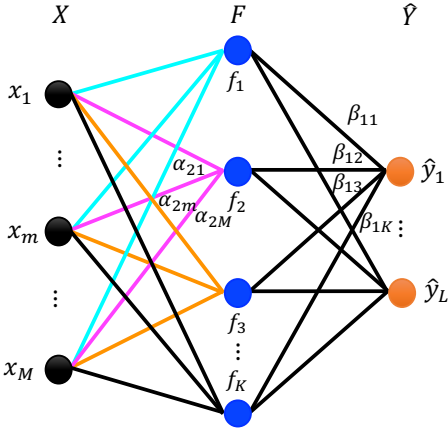


Fig. 3: The architecture of a shallow neural network. In the hidden layer F , each blue node is an activation function $f_k^{act}(\cdot)$, the lines with different colors indicate different linear filters $f_k(\cdot)$.

β_{lk} denote the weights. In addition, the partition function is defined as $Z = \sum_{\mathbf{X}} \exp\{\sum_{k=1}^K \beta_{lk} \cdot f_k^{act}(f(\mathbf{x}))\}$.

We can obtain that \hat{Y} is a Gibbs distribution of \mathcal{X} through comparing Equation (7) and (1). Specifically, \hat{Y} assumes that \mathcal{X} includes L states $\{\hat{y}_1, \dots, \hat{y}_L\}$ and the energy of each state is $g_l(\mathbf{x}) = \sum_{k=1}^K \beta_{lk} \cdot f_k^{act}[f_k(\mathbf{x})]$. In particular, $g_l(\mathbf{x})$ is a linear combination of all neurons in F .

We can also derive that F formulates a Gibbs distribution $p(F)$ of \mathcal{X} based on Equation (1). Similarly, F assumes that \mathcal{X} includes K states $\{F_1, \dots, F_K\}$ and the energy of each state is defined as $g_k(\mathbf{x}) = f_k^{act}[f_k(\mathbf{x})]$. Therefore, $p(F)$ can be expressed as follows.

$$p(F_k) = \frac{1}{Z_F} \exp\{f_k^{act}[f_k(\mathbf{x})]\} \quad (8)$$

Overall, the hidden layer F defines the energy function $g_k(\mathbf{x})$ of $p(F_k)$. Since the energy function is a sufficient statistics of the Gibbs distribution $p(F_k)$ [44], we can conclude that the hidden layers of a neural network are equivalent to Gibbs distributions of the network input.

Also note that the hidden layer defined in the network $\{\mathcal{X}; F; \hat{Y}\}$ is a fully connected layer, which assumes that there are finite K states in \mathcal{X} and uses the finite K states to formulate a discrete Gibbs distribution of \mathcal{X} . However, a discrete Gibbs distribution cannot explain the convolutional layer appropriately, since the output of a convolutional filter is a high-dimensional matrix, rather than a scalar to indicate the weight of a state. Alternatively, a convolutional layer with one or more non-linear layers can be formulated as a MRFs expressed as follows

$$p(\mathbf{x}; \theta) = \frac{1}{Z(\theta)} \exp\{\sum_{k=1}^K [f_k^{NL}(f_k(\mathbf{x}); \theta_k)]\} \quad (9)$$

where $f_k(\cdot)$ is the convolutional filter and $f_k^{NL}(\cdot)$ represent non-linear layers, such as ReLU or Max pooling layer.

Similarly, we can prove that Proposition 1 holds for all hidden layers by redefining linear filter $f_k(\cdot)$ and non-linear function $f_k^{NL}(\cdot)$ based on Equation (8) or Equation (9).

B. A Statistical Representation of DNNs

Proposition 2: the whole architecture of DNNs can be interpreted as a Bayesian Hierarchical Model (BHM).

Since the input of a hidden layer in DNNs is typically the output of its previous layer, it is more rational to state that a single hidden layer of DNNs defines a conditional Gibbs distribution given the previous layer based on Proposition 1.

Assuming there is a DNNs = $\{\mathcal{X}; F_1; \dots; F_I; \hat{Y}\}$, the distribution of F_i can be formulated a conditional Gibbs distribution $p(F_i|F_{i-1})$ as Equation (8) or (9) depending on the functionality of F_i . Without loss of generality, $p(F_1|\mathcal{X})$ can be expressed as $p(F_1)$, since \mathcal{X} will be replaced by \mathcal{X} , which is deterministic.

It has been proven that the DNNs = $\{\mathcal{X}; F_1; \dots; F_I; \hat{Y}\}$ form a Markov chain expressed below [45], [46],

$$\mathcal{X} \rightarrow F_1 \rightarrow \dots \rightarrow F_I \rightarrow \hat{Y} \quad (10)$$

the distribution of DNNs thus can be formulated as follows.

$$p(F_1; \dots; F_I; \hat{Y}) = p(F_1) \cdot \dots \cdot p(F_{i+1}|F_i) \cdot \dots \cdot p(\hat{Y}|F_I) \quad (11)$$

The above distribution shows that the DNNs can be interpreted as a BHM with $I + 1$ levels, in which F_i formulates a conditional Gibbs distribution to process the features in F_{i-1} and serves as a prior distribution for the higher level F_{i+1} .

Moreover, Bayes' theorem suggests that the above joint distribution of DNNs (Equation (11)) can be decomposed into two components: a prior distribution $p(\mathcal{X})$ and a likelihood distribution $p(\hat{Y}|\mathcal{X})$ expressed as follows.

$$p(F_1; \dots; F_I; \hat{Y}) = \underbrace{p(F_1) \cdot \dots \cdot p(F_{i-1}|F_{i-2})}_{\text{prior}} \cdot \underbrace{p(F_i|F_{i-1}) \cdot \dots \cdot p(\hat{Y}|F_I)}_{\text{likelihood}} \quad (12)$$

That above equation suggests that DNNs utilize some hidden layers (i.e., $F_1 \dots F_{i-1}$) to learn $p(\mathcal{X})$ and the other layers (i.e., $F_i \dots \hat{Y}$) are trained to learn $p(\hat{Y}|\mathcal{X})$ from \mathcal{X} and \mathcal{Y} .

In summary, the proposed framework establishes an explicit correspondence between DNNs and statistical models in three aspects: (i) neuron defines the energy of Gibbs distribution; (ii) the hidden layers of DNNs formulate Gibbs distributions; (iii) the whole architecture of DNNs can be interpreted as a BHM. In particular, this statistical framework provides a novel Bayesian perspective to understand the architecture of DNNs.

IV. THE INSIGHTS INTO DNNs

Based on the proposed statistical framework of DNNs, we specifies the application scope of DNNs, reveals a limitation of DNNs for CS restoration, establishes an overall picture of all existing BCS algorithms, and provides more explanation for the vulnerability of DNNs.

A. The Application Scope of DNNs

Based on Data Processing Inequality (DPI) [44], the Markov chain corresponding to the DNNs (Formula (10)) implies

$$H(\mathcal{X}) \geq I(\mathcal{X}, F_1) \cdot \dots \geq I(\mathcal{X}, \hat{Y}) \quad (13)$$

where $H(\mathcal{X})$ is the entropy of \mathcal{X} and $I(\mathcal{X}, \hat{Y})$ is the mutual information between \mathcal{X} and \hat{Y} .

The above inequality suggests that the information of DNNs input is great or equal to the output, which means that the application scope of DNNs is confine to the situation that \mathcal{X} provides great or equal to the information of \mathcal{Y} . In terms of Bayesian hierarchical model, DNNs formulate the prior knowledge of \mathcal{X} as a prior distribution $p(\mathbf{X})$ and establish an efficient representation of the output $p(\hat{\mathbf{Y}}|\mathbf{X})$ based on the extracted prior knowledge. Therefore, DNNs cannot learn an expressive Bayesian hierarchical model to derive the output unless the training dataset provides enough prior knowledge.

B. A Limitation of DNNs for CS restoration

Assuming there is a DNNs = $\{\mathbf{Y}; \mathbf{F}_1; \dots; \mathbf{F}_I; \hat{\mathbf{X}}\}$ designed for CS restoration, where \mathbf{Y} is the CS measurement and $\hat{\mathbf{X}}$ is the restored signal, We can derive that the DNNs formulate a Bayesian hierarchical model $p(\hat{\mathbf{X}}, \mathbf{Y}) = p(\mathbf{Y})p(\hat{\mathbf{X}}|\mathbf{Y})$. However, the DNNs cannot extract much prior knowledge of \mathbf{X} from \mathbf{Y} since \mathbf{Y} is compressed measurement. Therefore, we cannot achieve the state-of-the-art performance through simply applying DNNs to CS restoration.

Since ReconNet is a specific DNNs for CS restoration (Fig. 1), this limitation explains why it cannot outperform traditional BCS methods. Moreover, we can conclude that LDAMP achieves better restoration because it circumvents this limitation. Specifically, the AMP algorithm derives the preliminary restoration \mathbf{X}_p that provides much more prior knowledge of \mathbf{X} than \mathbf{Y} for LDAMP deriving $\hat{\mathbf{X}}$, which results in better restoration.

C. A Reason for the Vulnerability of DNNs

The vulnerability of DNNs implies that DNNs misclassify the input with small perturbations that are imperceptible to humans [47], [48]. The most widely accepted explanation for the vulnerability of DNNs is that the linear operators like convolutional filters magnify the perturbations, especially when the input is high-dimensional [47].

We discover another reason for the vulnerability of DNNs, i.e., the commonly used activation functions cannot denoise very well. Fig. 4 shows the spectrum of three activation functions. On the one hand, it shows that ReLU has the highest magnitude spectrum in all frequencies, hence ReLU can preserve the information of various features very well. On the other hand, the spectrum implies that ReLU has the worst ability of denoising. In contrast, GMM, as a popular statistical model in image denoising field [20], [18], achieves a tradeoff. Fig. 4 shows that GMM has high magnitude spectrum at low frequencies and the lowest magnitude at high frequencies, which indicates that GMM can preserve feature information and implement denoising simultaneously.

Since the perturbation is typically viewed as noise, the vulnerability of DNNs has great effect on the performance of DNNs for CS restoration. However, the most effective solution, namely adversarial training [47], [49], cannot improve the robustness of DNNs for CS restoration, since the variance of noise is unknown and varies in different CS applications such that we cannot train a DNNs for CS restoration in advance. Therefore, designing new activation function is an alternative way to improve the robustness of DNNs for CS restoration.

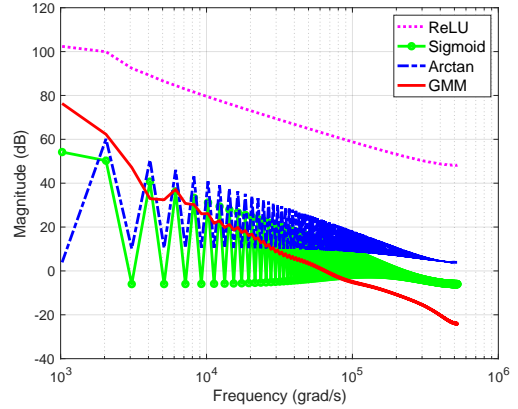


Fig. 4: The magnitude spectrum of three popular activation functions, where Arctan indicates the arctangent function. As a comparison, GMM is short for Gaussian Mixture Model.

D. An Overall Picture of BCS Algorithms

We can divide all BCS algorithms into four categories depending on how to model the prior distribution $p(\mathbf{x})$ and likelihood distribution $p(\mathbf{y}|\mathbf{x})$ in Table I, where \mathbf{x} is the original signal and \mathbf{y} is the CS measurement. The first uses traditional distributions to model both $p(\mathbf{x})$ and $p(\mathbf{y}|\mathbf{x})$, e.g., traditional BCS [8]. In contrast, the fourth category utilizes networks to estimate both $p(\mathbf{x})$ and $p(\mathbf{y}|\mathbf{x})$, e.g., ReconNet [25]. The third category uses networks to estimate the prior knowledge of \mathbf{x} and uses statistical methods to model the connection between \mathbf{x} and \mathbf{y} , e.g., LDAMP [29]. To the best of our knowledge, there is no algorithm belongs to the second category. The categorization unifies traditional BCS methods and DNNs and provides an overall picture of BCS.

In summary, all existing BCS algorithms have limitations. The first cannot describe the prior knowledge of \mathbf{x} precisely and comprehensively due to the limitation of traditional prior distributions discussed in Section II-B. The fourth cannot achieve the state-of-the-art CS restoration because of the limitation of DNNs discussed in Section IV-B. Though the third circumvents the limitation of DNNs, the vulnerability of DNNs affects its performance in noisy situations.

V. BAYESIAN CNNs METHOD FOR CS RESTORATION

This section describes a novel Bayesian CNNs (BCNNs) algorithm for CS restoration. First, we propose a novel CNNs to model the prior distribution $p(\mathbf{x}; \boldsymbol{\theta})$ only. Given the prior distribution $p(\mathbf{x}; \boldsymbol{\theta})$ corresponding to the CNNs, we derive the corresponding posterior distribution via the likelihood distribution of CS. Finally, we propose a novel Bayesian inference algorithm based on auxiliary variable Gibbs sampler to infer the posterior distribution for CS restoration.

TABLE I: Four Categories of BCS Algorithms

Category	Prior	Likelihood	Example
1	statistics	statistics	BCS[8]
2	statistics	networks	None
3	networks	statistics	LDAMP[29]
4	networks	networks	ReconNet[25]

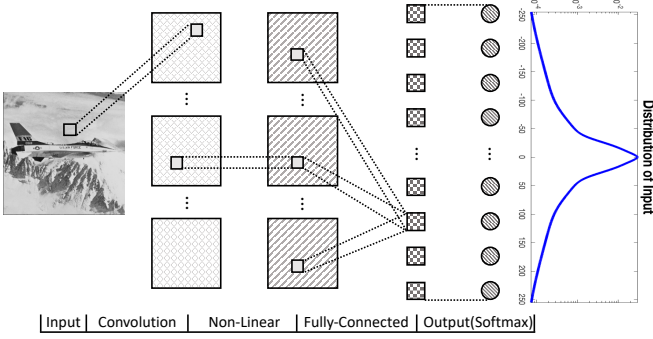


Fig. 5: The architecture of the proposed CNNs for modeling a prior distribution $p(\mathbf{x}; \theta)$ like the curve depicted in the right.

A. A New Approach to Design DNNs for CS Restoration

Unlike previous works designing an end-to-end DNNs to derive CS restoration directly, we propose a novel CNNs to model a prior distribution $p(\mathbf{x}; \theta)$ only, which brings three advantages over the existing DNNs for CS restoration: (i) we can use high-dimensional dataset rather than CS measurement as the training dataset, which guarantees the proposed CNNs can extract enough prior knowledge to learn an expressive $p(\mathbf{x}; \theta)$; (ii) we can decrease the complexity of networks, since the proposed CNNs only simulate the prior distribution $p(\mathbf{x}; \theta)$; (iii) we can design new activation function to improve the robustness of the DNNs based on Proposition 1.

Given the $p(\mathbf{x}; \theta)$ generated from the proposed CNNs, we can derive the corresponding posterior distribution via the likelihood distribution of CS, and CS restoration can be achieved by inferring the posterior distribution.

B. The Architecture of The Proposed CNNs

The architecture of the proposed CNNs is depicted in Fig. 5, which includes three hidden layers: convolutional, non-linear (i.e., activation function), and fully connected layers. The output layer is defined as softmax, and the corresponding prior distribution $p(\mathbf{x}; \theta)$ can be formulated as

$$p(\mathbf{x}; \theta) = \frac{1}{Z(\theta)} \exp\left\{\sum_{m=1}^M (f_m^{NL}(f_m(\mathbf{x})))\right\} \quad (14)$$

where $f_m(\cdot)$ and $f_m^{NL}(\cdot)$ are convolutional filter and activation function, respectively. $\sum_{m=1}^M (f_m^{NL}(f_m(\mathbf{x})))$ represents the fully-connected layer.

Since GMM demonstrates better denoising ability than most popular activation functions, $f_m^{NL}(\cdot)$ is chosen as GMM to improve the robustness of the proposed CNNs. It is formulated as $f_m^{NL}(\cdot) = \log[\sum_{n=1}^N \pi_{mn} \cdot \mathcal{N}(f_m(\cdot); 0, \sigma_b^2/\delta_n)]$, where σ_b^2 is a fixed base variance, $\delta = \{\delta(1), \dots, \delta(N)\}$ is a range of constant scales, and π_{mn} denotes the weight of each Gaussian distribution. Therefore, the $p(\mathbf{x}; \theta)$ corresponding to the proposed CNNs can be formulated as

$$p(\mathbf{x}; \theta) = \frac{1}{Z(\theta)} \prod_{m=1}^M \sum_{n=1}^N \pi_{mn} \cdot \mathcal{N}(f_m(\mathbf{x}); 0, \frac{\sigma_b^2}{\delta(n)}) \quad (15)$$

Overall, the proposed CNNs formulates a prior distribution, in which the convolutional layer learn the features from the training dataset, and the activation function is defined as GMM to introduce non-linearity and implement denoising.

Algorithm 1 CNNs learning algorithm for prior distribution

input: training data TD , CNNs model

- 1: **initialize**
 - 2: GSM scales δ_n , base variance σ_b^2
 - 3: CNNs parameters $\theta = \{\mathbf{f}, \boldsymbol{\pi}\}$
 - 4: sampling iteration k
 - 5: training iteration count $n = 0$
 - 6: training parameters, e.g., learning rate η , batch size.
 - 7: **repeat**
 - 8: prepare training batch TB_n from TD
 - 9: compute $\langle \nabla CNN \rangle_{p(\mathbf{x}^{data}; \theta_n)}$ based on TB_n
 - 10: obtain training label TL_n via sampling $p(\mathbf{x}_k^{prior}; \theta_n)$
 - 11: compute $\langle \nabla CNN \rangle_{p(\mathbf{x}_k^{prior}; \theta_n)}$ based on TL_n
 - 12: update θ_n based on gradient descent method (17)
 - 13: $n \leftarrow n + 1$
 - 14: **until** ($|\theta_{n+1} - \theta_n| < \xi$ or $n > N$)
- output:** optimal parameter $\theta^* = \theta_n$

After specifying the CNNs architecture, the next problem is to construct the learning algorithm to optimize $\theta = \{\mathbf{f}, \boldsymbol{\pi}\}$, where $\mathbf{f} = [f_1, \dots, f_m]$ and $\boldsymbol{\pi} = [\pi_{11}, \dots, \pi_{NM}]$. Here we choose Kullback-Leibler divergence (KLD) [50] as the criterion to measure the distance between $p(\mathbf{x}^{prior}; \theta)$ and $p(\mathbf{x}^{data}; \theta)$. KLD is defined as

$$\text{KLD}(p(\mathbf{x}^{prior}; \theta) || p(\mathbf{x}^{data}; \theta)) = \sum_i p(\mathbf{x}^{data}(i); \theta) \cdot \log \frac{p(\mathbf{x}^{data}(i); \theta)}{p(\mathbf{x}^{prior}(i); \theta)} \quad (16)$$

where $p(\mathbf{x}^{prior}; \theta)$ is the stationary distribution generated by sampling $p(\mathbf{x}; \theta)$, and $p(\mathbf{x}^{data}; \theta)$ denotes the empirical distribution of the training dataset, namely the output of the proposed CNNs. In order to make $p(\mathbf{x}; \theta)$ model the statistical property of the training dataset as precisely as possible, the KLD should be minimized, which can be realized by gradient descent algorithm [50].

In practice, it is time-consuming to obtain $p(\mathbf{x}^{prior}; \theta)$ by sampling $p(\mathbf{x}; \theta)$ continuously until stationary. Therefore, Contrastive Divergence (CD) learning method [51] is adopted to quickly optimize $\theta = \{\mathbf{f}, \boldsymbol{\pi}\}$, and it can be formulated as

$$\theta_{n+1} = \theta_n - \eta \cdot [\langle \nabla CNN \rangle_{p(\mathbf{x}_k^{prior}; \theta_n)} - \langle \nabla CNN \rangle_{p(\mathbf{x}^{data}; \theta_n)}] \quad (17)$$

where θ_n denote the optimized parameters at the n th training epoch, $\nabla CNN = \frac{\partial \log(p(\mathbf{x}, \theta))}{\partial \theta}$, $\langle \cdot \rangle_p$ indicates the average over p , and $\eta \in (0, 1]$ denotes the learning rate.

Since CD learning algorithm only takes few k sampling iterations to estimate $p(\mathbf{x}; \theta)$, it can increase training speed greatly while guarantee similar training result. In summary, the learning algorithm for the proposed CNNs is presented in Algorithm 1.

C. Bayesian CNNs Inference for CS restoration

In the framework of traditional BCS, we need derive the posterior distribution $p(\mathbf{x} | \mathbf{A}, \mathbf{y}, \mathbf{z}, \sigma_n^2; \theta)$ based on the prior distribution $p(\mathbf{x}; \theta)$ and the likelihood distribution $p(\mathbf{y} | \mathbf{x}, \mathbf{A}, \sigma_n^2)$ for CS restoration. However, the $p(\mathbf{x}; \theta)$ is intractable for most conventional inference algorithms [34]. Alternatively, we utilize auxiliary variable Gibbs sampler to simplify the $p(\mathbf{x}; \theta)$ for deriving an applicable posterior inference algorithm [19], [52].

Algorithm 2 Bayesian CNNs algorithm for CS restoration

input: \mathbf{y} , \mathbf{A} , $p(\mathbf{x}; \boldsymbol{\theta})$, and $p(\mathbf{y}|\mathbf{x}, \mathbf{A}, \sigma_n^2)$

- 1: **initialize**
- 2: randomly initialize \mathbf{x} , \mathbf{z} , σ_n^2
- 3: sampling iteration n
- 4: **repeat**
- 5: sampling $p(z_{mn}|\mathbf{x}; \boldsymbol{\theta})$
- 6: sampling $p(\mathbf{x}|\mathbf{A}, \mathbf{y}, \mathbf{z}, \sigma_n^2; \boldsymbol{\theta})$
- 7: sampling $p(\sigma_n^2|\mathbf{x}, \mathbf{y}, \mathbf{A}) = \text{Gamma}(\frac{M}{2} + 1, \frac{2}{\|\mathbf{y} - \mathbf{A}\mathbf{x}\|^2})$
- 8: $n \leftarrow n - 1$
- 9: **until** ($n = 0$)

output: recovery signal $\mathbf{x}^* = \mathbf{x}$

Since GMM can be viewed as a discrete case of GSM model [53], which is defined as

$$p(\mathbf{x}, \mathbf{z}) = \int_{-\infty}^{\infty} \frac{1}{2\pi|\mathbf{z}|^2 \Sigma^{1/2}} \exp\left(-\frac{\mathbf{x}^T \Sigma^{-1} \mathbf{x}}{2z^2}\right) \cdot p(z) dz \quad (18)$$

where \mathbf{z} denotes an auxiliary random vector $\mathbf{z} \in \{1, \dots, N\}^M$ to represent the scale δ_n , the $p(\mathbf{x}; \boldsymbol{\theta})$ can be augmented into a joint distribution $p(\mathbf{x}, \mathbf{z}; \boldsymbol{\theta})$.

Furthermore, two conditional distributions $p(\mathbf{x}|\mathbf{z}; \boldsymbol{\theta})$ and $p(\mathbf{z}|\mathbf{x}; \boldsymbol{\theta})$ corresponding to $p(\mathbf{x}, \mathbf{z}; \boldsymbol{\theta})$ can be derived below.

$$p(z_{mn}|\mathbf{x}; \boldsymbol{\theta}) \propto \pi_{mn} \cdot \mathcal{N}(f_m(\mathbf{x}); 0, \frac{\sigma_b^2}{\delta_n}) \quad (19)$$

$$p(\mathbf{x}|\mathbf{z}; \boldsymbol{\theta}) \propto \prod_{m=1}^M \mathcal{N}(f_m(\mathbf{x}); 0, \frac{\sigma_b^2}{z_m}) \quad (20)$$

Ultimately, the posterior distribution $p(\mathbf{x}|\mathbf{A}, \mathbf{y}, \mathbf{z}, \sigma_n^2; \boldsymbol{\theta})$ of CS can be formulated below based on (20) and (4).

$$p(\mathbf{x}|\mathbf{A}, \mathbf{y}, \mathbf{z}, \sigma_n^2; \boldsymbol{\theta}) \propto \prod_{m=1}^M \mathcal{N}(f_m(\mathbf{x}); 0, \frac{\sigma_b^2}{z_m}) \cdot p(\mathbf{y}|\mathbf{x}, \mathbf{A}, \sigma_n^2) \quad (21)$$

Since all f_m and \mathbf{A} are linear, $p(\mathbf{x}|\mathbf{A}, \mathbf{y}, \mathbf{z}, \sigma_n^2; \boldsymbol{\theta})$ can be rewritten in matrix form to get more intuitive expression.

$$p(\mathbf{x}|\mathbf{A}, \mathbf{y}, \mathbf{z}, \sigma_n^2; \boldsymbol{\theta}) \propto \exp\{-\mathbf{F}\mathbf{x} - \boldsymbol{\mu}\}^T \boldsymbol{\Sigma}^{-1} \{\mathbf{F}\mathbf{x} - \boldsymbol{\mu}\} \quad (22)$$

where

$$\mathbf{F} = \begin{bmatrix} \mathbf{f}_1 \\ \vdots \\ \mathbf{f}_m \\ \mathbf{A} \end{bmatrix}; \boldsymbol{\Sigma} = \begin{bmatrix} \frac{\sigma_b^2}{z_1} \mathbf{I} & \dots & \mathbf{0} & \mathbf{0} \\ \vdots & \ddots & \mathbf{0} & \vdots \\ \mathbf{0} & \dots & \frac{\sigma_b^2}{z_M} \mathbf{I} & \mathbf{0} \\ \mathbf{0} & \dots & \mathbf{0} & \sigma_n^2 \mathbf{I} \end{bmatrix}; \boldsymbol{\mu} = \begin{bmatrix} \mathbf{0} \\ \vdots \\ \mathbf{0} \\ \mathbf{y} \end{bmatrix}$$

We can find that Equation (22) is a Gaussian distribution, such that CS restoration can be inferred through alternately sampling $p(\mathbf{x}|\mathbf{A}, \mathbf{y}, \mathbf{z}, \sigma_n^2; \boldsymbol{\theta})$ and $p(\mathbf{z}|\mathbf{x}; \boldsymbol{\theta})$ in Algorithm 2.

VI. EXPERIMENTAL RESULTS

This section presents our experimental results. First, BCNNs are evaluated in CS image restoration field given different hyper-parameters. Second, BCNNs are compared to the state-of-the-art CS restoration algorithms in noiseless and noisy situations. BCNNs are implemented by MATLAB. All related simulation code, training dataset are available online¹.

¹Available at <https://github.com/EthanLan/BCNN>

A. Experimental Setup

There are three hyper-parameters of BCNNs: convolutional depth F_n (i.e., the number of convolutional filters f_m), filter dimension \mathcal{N}_d , and GSM scales $\boldsymbol{\delta}$ need to initialize.

To evaluate the influence of different hyper-parameters on BCNNs, we instantiate five models of BCNNs, and they are summarized in Table II. For example, BCNN2 has four convolutional filters, i.e., $F_n = 4$, and the dimension of each filter is defined as \mathcal{N}_2 . The scales $\boldsymbol{\delta}$ of BCNN2 are initialized as $\boldsymbol{\delta}_1$. Therefore, BCNN2 can be formulated as follows.

$$p(\mathbf{x}; \boldsymbol{\theta}) = \frac{1}{Z(\boldsymbol{\theta})} \prod_{m=1}^4 \sum_{n=1}^5 \pi_{mn} \cdot \mathcal{N}(f_m(\mathbf{x}); 0, \frac{\sigma_b^2}{\delta_1(n)}) \quad (23)$$

We can derive that BCNN2 has 56 parameters need to learn, i.e., $|\boldsymbol{\theta}| = F_n \times |f_m| + |\boldsymbol{\pi}| = 56$, where $|f_m|$ and $|\boldsymbol{\pi}|$ denote the number of parameters of f_m and π_{mn} , respectively. Table II shows that larger \mathcal{N}_d , F_n , or $\boldsymbol{\delta}$ requires more parameters, hence $|\boldsymbol{\theta}|$ can indicate the complexity of each model.

TABLE II: BCNNs Models with Different Hyper-parameters

Model	\mathcal{N}_d	F_n	$\boldsymbol{\delta}$	$ \boldsymbol{\theta} $
BCNN1	\mathcal{N}_1	4	$\boldsymbol{\delta}_1$	40
BCNN2	\mathcal{N}_2	4	$\boldsymbol{\delta}_1$	56
BCNN3	\mathcal{N}_2	8	$\boldsymbol{\delta}_1$	113
BCNN4	\mathcal{N}_2	8	$\boldsymbol{\delta}_2$	136
BCNN5	\mathcal{N}_3	24	$\boldsymbol{\delta}_2$	792

\mathcal{N}_1 means a filter only includes the nearest four neighbors.

\mathcal{N}_2 is 3×3 filter, and \mathcal{N}_3 is 5×5 filter.

$\boldsymbol{\delta}_1 = \{\exp(-7, -3, 0, 3, 7)\}$, $\boldsymbol{\delta}_2 = \{\exp(\pm 7, \pm 5, \pm 3, \pm 1)\}$.

Six recently developed CS restoration methods: LASSO², SSM³, TV⁴, ReconNet⁵, DR2Net⁶, and LDAMP⁷ are chosen as references. LASSO is a well-known CS restoration algorithm [54]. SSM is a BCS method integrating the cluster structure in \mathcal{N}_1 dimension by formulating the prior distribution as the Spike and Slab Model (SSM) defined below [15].

$$p(\mathbf{x}) = (1 - \pi)\delta_0 + \pi\mathcal{N}(\mathbf{x}; 0, \sigma^2) \quad (24)$$

where δ_0 is the Dirac function centered at zero, and π is commonly extended to a linear filter to describe the cluster structure. As a counterpart, TV is a deterministic CS method to include the same signal structure as SMM [55].

ReconNet, DR2Net and LDAMP are three DNNs designed for CS restoration. For a fair comparison, the refining networks of DR2Net and LDAMP are redesigned to keep the same as ReconNet except for some necessary layers for the residual technique. In other words, the refining networks of the three DNNs have six convolutional layers with the same convolutional filters and six ReLU layers depicted in Fig. 1.

The same training dataset of ReconNet and DR2Net are used to train BCNNs and LDAMP, which consists of 91 natural images. We uniformly extract 21,668 20×20 image patches from this dataset for training. Peak Signal-to-Noise Rate (PSNR), Structural Similarity Index (SSIM), and KLD are chosen as the quantitative criteria.

²Available at <http://sparselab.stanford.edu/>

³Available at <https://sites.google.com/site/link2yulei/publications>










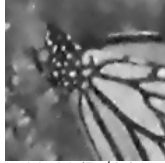
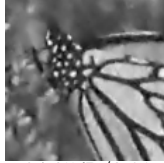
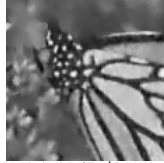









⁴Available at <http://www.caam.rice.edu/~optimization/L1/TV/L3/>

⁵Available at <https://github.com/KuldeepKulkarni/ReconNet>

⁶Available at https://github.com/coldrainyht/caffe_dr2/tree/master/DR2

⁷Available at https://github.com/ricedsp/D-AMP_Toolbox

TABLE III: BCNNs Restoration Performance [PSNR/SSIM] Given Different Hyper-parameters

Original	SSM	BCNN1	BCNN2	BCNN3	BCNN4	BCNN5
 Starfish	 21.28dB/0.58	 22.42dB/0.64	 23.98dB/0.74	 24.37dB/0.76	 24.45dB/0.77	 24.56dB/0.77
 Butterfly	 19.54dB/0.58	 22.61dB/0.75	 24.05dB/0.81	 24.40dB/0.82	 24.59dB/0.82	 24.80dB/0.84
 Parrot	 20.87dB/0.56	 25.32dB/0.82	 25.92dB/0.84	 26.53dB/0.85	 26.72dB/0.85	 26.61dB/0.84

B. Evaluation of BCNNs for CS restoration

Since the $p(\mathbf{x}; \boldsymbol{\theta})$ plays a vital role in CS restoration, we first evaluate the ability of BCNNs to model $p(\mathbf{x}; \boldsymbol{\theta})$ given different hyper-parameters. We compare the KLD between an empirical distribution and the samples of five BCNN models. The empirical distribution (the red curve in Fig. 6) is generated from a testing dataset including 20 image patches randomly chosen from the training dataset. The samples of five BCNN models are generated by sampling the $p(\mathbf{x}; \boldsymbol{\theta})$.

Fig. 6(a) shows that BCNN1 has the highest KLD (0.245). That means it has the worst ability to model the empirical distribution. BCNN2 has smaller KLD (0.156) than BCNN1, since it enlarges \mathcal{N}_1 to \mathcal{N}_2 while remaining the value of F_n and δ the same as BCNN1. Increasing F_n from 4 to 8

makes BCNN3 get smaller KLD (0.126) than BCNN2. Fig. 6(c) shows that the KLD (0.108) of BCNN4 is less than BCNN3 since the former has more GSM scales than the later. BCNN5 achieves the smallest KLD (0.089), because we increase \mathcal{N}_d and F_n both. In summary, the model with more hyper-parameters has smaller KLD, which means that it can simulate the empirical distribution better.

Subsequently, the above BCNNs models are evaluated by grayscale image restoration, and SSM is selected as baseline here. Gaussian random matrix is used to obtain the measurement \mathbf{y} from three standard test images (starfish, butterfly, and parrot), and image dimension is 128×128 . Measurement ratio ($MR = |\mathbf{y}|/|\mathbf{x}|$) is 0.25, so the dimension of \mathbf{y} is 4096×1 , where $|\mathbf{x}| = 128^2$ is the cardinality of \mathbf{x} . The performance of five BCNNs models are posted in Table III, which shows that all BCNNs models outperform SSM and the model with lower KLD achieves better restoration in most cases.

The superiority of BCNNs can be ascribed to three reasons. First, BCNNs can derive optimal parameters by the efficient training algorithm. For example, though BCNN1 employs the same \mathcal{N}_1 filters as SSM to simulate the cluster structure, BCNN1 can learn optimal convolutional filters $f_m(\cdot)$ via CD learning algorithm but SSM merely uses hand-crafted filters. Moreover, BCNN1 can learn optimal weights π_{mn} of GMM to preserve non-linearity precisely, which is also very difficult to realize by traditional Bayesian inference method [19].

Second, BCNNs can accommodate arbitrary convolutional filters in the architecture of CNNs. More convolutional filters can describe more signal structures, thereby achieving better CS restoration. But most prior distributions can only adopt few filters because of their limitations discussed in Section II-B. For instance, SSM merely incorporates four linear filters to describe the cluster structure, which is not enough to achieve the state-of-the-art CS restoration. In contrast, the number of linear filters in BCNN3 is twice as many as SSM. Hence, BCNN3 can achieve better restoration.

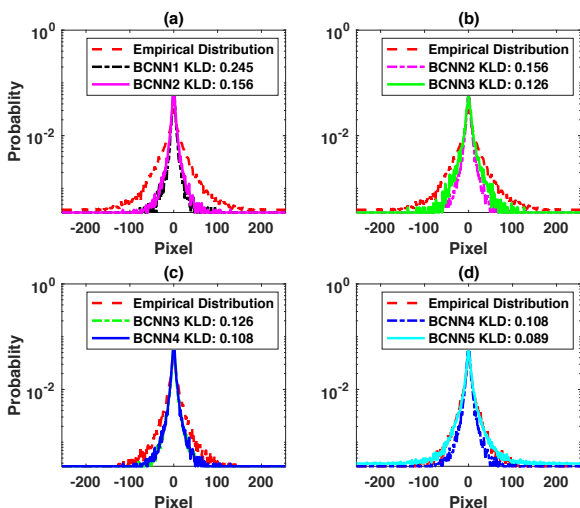









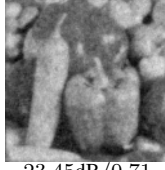


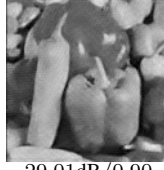










Fig. 6: (a) the influence of increasing \mathcal{N}_1 to \mathcal{N}_2 , (b) the influence of increasing F_4 to F_8 , (c) the influence of increasing δ_1 to δ_2 , (d) the influence of increasing \mathcal{N}_d and F_n both.

TABLE IV: Restoration Comparison [PSNR/SSIM] in Noiseless Situation

Original	SSM	TV	ReconNet	DR2Net	LDAMP	BCNNs
						
Plane	22.06dB/0.59	23.19dB/0.62	22.23dB/0.65	23.89dB/0.70	27.23dB/0.80	27.47dB/0.86
						
Peppers	21.79dB/0.61	23.45dB/0.71	23.00dB/0.73	25.17dB/0.78	29.01dB/0.90	29.73dB/0.90
						
Boat	23.10dB/0.58	24.78dB/0.68	23.50dB/0.68	25.14dB/0.73	26.91dB/0.89	26.61dB/0.86

Third, BCNNs can accommodate complicated convolution filters. Most prior distributions can only model the signal structure in a small neighborhood, e.g., SSM merely describes the cluster structure in \mathcal{N}_1 , which is hard to model high-order cluster structures. Compared to SSM, BCNNs can use more complicated filters to describe high-order structures. Fig. 7 draws all convolutional filters of BCNN4 and BCNN5, which shows that they can learn more complex signal structures than SSM. That helps them to generate more powerful prior distributions and achieve much better CS restoration.

Notably, the superiority of BCNN5 over BCNN4 is not very striking, even though the former has more complex networks. That is because BCNN4 has already captured most signal structures for CS restoration. Though BCNN5 can learn more complex signal structures, but these learned signal structures can not provide much more information for CS restoration. Fig. 7 shows that some filters of BCNN5 are similar as BCNN4, e.g., Filter 4 of BCNN4 and Filter 16 of BCNN5. Furthermore, more complicated networks could make BCNN5 difficult to converge.

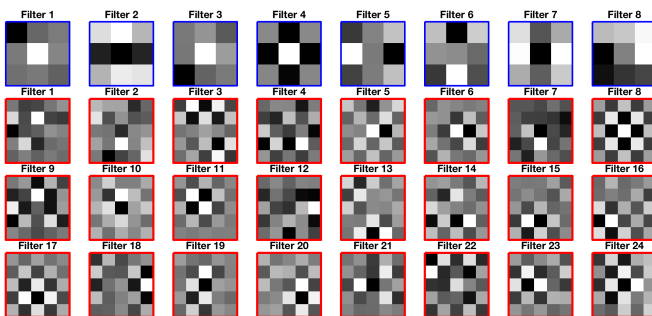


Fig. 7: The convolutional filters from BCNN4 and BCNN5. The first 8 filters with blue boundary belong to BCNN4, and the left 24 filters with red boundary belong to BCNN5.

C. Comparisons with Other Algorithms in Noiseless Situation

BCNN4 model is chosen to represent BCNNs algorithm for the following experiments, since it achieves the best tradeoff between network complexity and performance. First, the above CS restoration methods are tested by three standard grayscale images (plane, peppers, and boat) with $MR = 0.25$ under the same experimental conditions as above. Table IV shows that BCNN4 outperforms the traditional CS algorithms, i.e., TV and SSM, due to the advantages of BCNNs discussed above. BCNN4 also outperforms three DNNs algorithms, even though the former has much simpler architecture than the later.


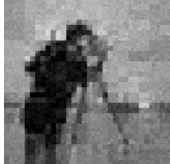






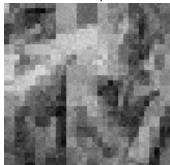
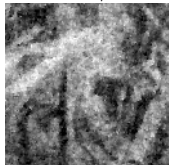
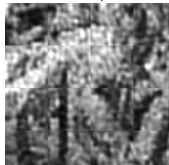
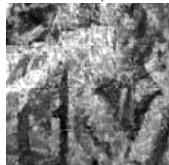
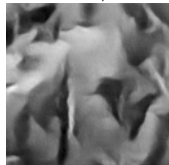


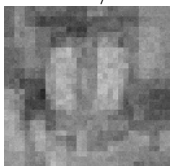
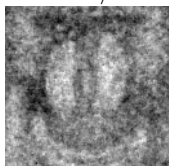
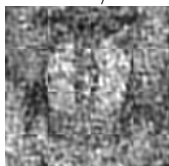
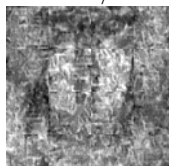
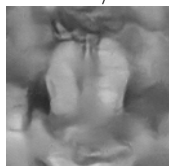
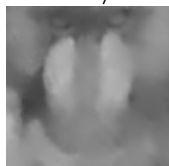
To further validate BCNNs, all algorithms are evaluated by a testing dataset, which has 50 images randomly selected from Berkeley Segmentation Dataset and Benchmark (BSDS) dataset [56], and every image is cropped into 128×128 . Given three different MRs ($MR = 0.25, 0.10, \text{ and } 0.04$), Table V summarizes their average performances in noiseless situation. It is noteworthy that BCNNs still outperform both traditional SCS and CNNs algorithms in all cases.

Also note that ReconNet does not outperform both SSM and TV algorithms, which validates the limitation of DNNs, i.e., simply applying DNNs to CS restoration cannot achieve the state-of-the-art performance, because CS measurement cannot provide enough prior knowledge for DNNs to formulate an expressive Bayesian hierarchical model.

TABLE V: CS Restoration in Noiseless Situation

Method	MR = 0.25		MR = 0.10		MR = 0.04	
	PSNR(dB)	SSIM	PSNR(dB)	SSIM	PSNR(dB)	SSIM
LASSO	12.15	0.03	13.18	0.01	13.99	0.01
BCS	25.06	0.65	22.23	0.49	20.12	0.37
TV	26.20	0.71	20.73	0.44	19.39	0.26
ReconNet	24.12	0.68	21.95	0.55	20.07	0.44
DR2Net	25.86	0.74	22.77	0.59	20.42	0.46
LDAMP	27.17	0.76	23.61	0.58	20.45	0.42
BCNNs	28.58	0.81	24.67	0.63	21.27	0.47

TABLE VI: Restoration Comparison [PSNR/SSIM] in Noisy Situation (SNR=12dB)

Original	SSM	TV	ReconNet	DR2Net	LDAMP	BCNNs
 Cameraman	 19.87dB/0.40	 19.36dB/0.33	 18.39dB/0.39	 18.50dB/0.34	 21.42dB/0.63	 21.56dB/0.67
 Barbara	 19.71dB/0.38	 19.24dB/0.46	 18.95dB/0.51	 19.07dB/0.49	 20.29dB/0.54	 21.30dB/0.58
 Mandrill	 21.53dB/0.38	 19.78dB/0.36	 18.53dB/0.32	 18.51dB/0.32	 22.08dB/0.43	 22.24dB/0.49

D. Comparisons with Other Algorithms in Noisy Situation

The CS restoration algorithms are first tested by three standard grayscale images (cameraman, barbara, and mandrill) in the noisy situation (SNR = 12dB) by adding Gaussian noise into CS measurement \mathbf{y} , and the other experimental conditions are the same as before. Table VI shows their performances. Furthermore, we use the same testing dataset from BSDS to further test these methods in two more noisy situations, i.e., SNR = 16dB and 8dB. Their average performances are presented in Table VII and Table VIII, respectively.

We can find that BCNNs still achieve the best performance in various noisy situations. ReconNet and DR2Net do not outperform traditional BCS method in noisy situation, due to the vulnerability of DNNs. Since LDAMP and BCNNs are hybrid algorithms of DNNs and traditional BCS, they are more robust and achieve better performance in noisy situation.

TABLE VII: CS Image Restoration with SNR=16dB

Method	MR = 0.25		MR = 0.10		MR = 0.04	
	PSNR(dB)	SSIM	PSNR(dB)	SSIM	PSNR(dB)	SSIM
LASSO	12.03	0.03	13.13	0.01	13.98	0.01
BCS	22.79	0.52	20.99	0.41	19.34	0.32
TV	22.86	0.51	19.89	0.38	17.02	0.24
ReconNet	21.39	0.51	20.26	0.44	18.62	0.35
DR2Net	21.93	0.52	20.77	0.46	18.91	0.37
LDAMP	22.81	0.54	20.66	0.45	18.45	0.33
BCNNs	23.54	0.64	21.96	0.51	19.95	0.40

TABLE VIII: CS Image Restoration with SNR=8dB

Method	MR = 0.25		MR = 0.10		MR = 0.04	
	PSNR(dB)	SSIM	PSNR(dB)	SSIM	PSNR(dB)	SSIM
LASSO	11.43	0.02	12.85	0.01	13.83	0.01
BCS	20.61	0.38	19.20	0.29	17.80	0.16
TV	17.45	0.26	17.47	0.25	16.03	0.18
ReconNet	16.08	0.29	16.35	0.28	15.18	0.23
DR2Net	16.19	0.28	16.67	0.27	15.23	0.23
LDAMP	18.89	0.33	17.07	0.30	16.58	0.22
BCNNs	21.11	0.46	19.32	0.37	17.79	0.31

E. Comparisons with Deeper Neural Networks

We design two new networks DR2Net-12 and LDAMP-12 to evaluate the effect of deeper refining networks. Compared to the refining networks of DR2Net only consisting of six convolutional layers, the refining networks of DR2Net-12 includes twelve convolutional layers. The difference between LDAMP-12 and LDAMP is the same.

Given the same experimental conditions as above, we presents the performances of DR2Net-12 and LDAMP-12 in Table IX and Table X. We can find that DR2Net-12 shows similar performance as DR2Net, which further validates the limitation of DNNs for CS restoration. Also note that LDAMP-12 achieves notable improvement over LDAMP and outperforms BCNNs in noiseless situation, but only shows similar performance as BCNNs in noisy situation. In summary, BCNNs still demonstrate effective and robust CS restoration compared to deeper neural networks in both noiseless and noisy situations.

TABLE IX: CS Restoration in Noiseless Situation

Method	MR = 0.25		MR = 0.10		MR = 0.04	
	PSNR(dB)	SSIM	PSNR(dB)	SSIM	PSNR(dB)	SSIM
DR2Net	25.86	0.74	22.77	0.59	20.42	0.46
DR2Net-12	26.49	0.76	22.97	0.61	20.47	0.48
LDAMP	27.17	0.76	23.61	0.58	20.45	0.42
LDAMP-12	29.58	0.82	24.70	0.63	21.69	0.53
BCNNs	28.58	0.81	24.67	0.68	21.27	0.47

TABLE X: CS Restoration with SNR = 8dB

Method	MR = 0.25		MR = 0.10		MR = 0.04	
	PSNR(dB)	SSIM	PSNR(dB)	SSIM	PSNR(dB)	SSIM
DR2Net	16.19	0.28	16.67	0.27	15.23	0.23
DR2Net-12	16.37	0.28	16.52	0.27	15.19	0.22
LDAMP	18.89	0.33	19.32	0.30	16.58	0.22
LDAMP-12	20.81	0.47	19.47	0.33	16.89	0.27
BCNNs	21.11	0.46	19.32	0.37	17.79	0.31

VII. CONCLUSION

In this paper, we attempt to propose a statistical framework to explain the architecture of DNNs and design a novel algorithm for CS restoration based on the proposed framework.

The proposed framework of DNNs demonstrates that (i) neuron defines the energy of Gibbs distribution; (ii) the hidden layers of DNNs formulate Gibbs distributions; (iii) the whole architecture of DNNs can be explained as a BHM. In particular, this statistical framework provides a novel Bayesian perspective to understand the architecture of DNNs.

Based on the proposed framework, we provide insights into DNNs in four aspects: (i) we specify the application scope of DNNs; (ii) we reveal a limitation of DNNs for CS restoration; (iii) we find that an important reason for the vulnerability of DNNs is the activation function of DNNs cannot denoise very well; (iv) we unify traditional BCS methods and DNNs and provide an overall picture of all BCS algorithms.

We propose a novel CS restoration algorithm based on DNNs. In contrast to design an end-to-end DNNs for CS restoration, we propose a novel CNNs to model a prior distribution $p(\mathbf{x}; \theta)$ only. The proposed CNNs have a dual property: (i) it has a closed-form expression as traditional prior distributions; (ii) it preserves the same powerful representation ability as DNNs. Based on the prior distribution $p(\mathbf{x}; \theta)$ corresponding to the CNNs and the likelihood distribution of CS, we derive the posterior distribution of CS and propose a novel Bayesian inference algorithm for CS restoration.

Extensive simulations validate the superiority of BCNNs over the state-of-the-art CS restoration methods. First, we show that BCNNs can learn a powerful prior distribution over traditional prior distributions, which is essential for traditional BCS algorithms. Second, BCNNs show effective performance than the existing CS restoration algorithms in noiseless and noisy situations. However, BCNNs are still not perfect. First, the speed of BCNNs is slower than the existing CS restoration algorithms, since the $p(\mathbf{x}; \theta)$ corresponding to the CNNs are so complex that the posterior inference algorithm is time consuming. Second, LDAMP with deeper refining networks can outperform BCNNs in noiseless situation.

There are numerous directions for future work. In terms of deep learning theory, the proposed framework of DNNs provides a new approach to solve the inherent problems of DNNs, such as proposing new DNNs architecture to defense the adversarial attacks in image classification field. In the context of CS restoration, our future work can include the following topics. First, we can refine the BCNNs algorithm to improve speed, which can extend the applications of BCNNs to real-time situations. Second, we can propose new BCNNs architecture consisting of deeper neural networks to improve its performance further.

ACKNOWLEDGMENT

The authors would like to thank Matiz Romero Sergio, Bayram Samet, and anonymous reviewers for their helpful comments and suggestions. This work is supported by the National Science Foundation under Grant No. 1319598.

REFERENCES

- [1] C. Shannon, "Communication in the presence of noise," *Proceedings of the IEEE*, vol. 72, pp. 1192–1201, 1984.
- [2] E. Candes and M. Wakin, "An introduction to compressive sampling," *IEEE Signal Pro. Mag.*, vol. 25, pp. 21–30, 2008.
- [3] D. Donoho, "Compressed sensing," *IEEE Trans. Info. Theory*, vol. 52, pp. 1289–1306, 2006.
- [4] T. Blumensath and M. E. Davies, "Sampling theorems for signals from the union of finite-dimensional linear subspaces," *IEEE Trans. Inf. Theory*, vol. 55, no. 4, pp. 1872–1882, 2009.
- [5] E. J. Cands, "The restricted isometry property and its implications for compressed sensing," *Comptes Rendus Mathematique*, vol. 52, pp. 589–592, 2008.
- [6] M. F. Duarte and Y. C. Eldar, "Structured compressed sensing: From theory to applications," *IEEE Trans. on Signal Proc.*, vol. 59, pp. 4053–4085, 2011.
- [7] R. G. Baraniuk, V. Cevher, M. F. Duarte, and C. Hegde, "Model based compressive sensing," *IEEE Trans. on Inf. theory*, vol. 56, pp. 1982–2001, 2010.
- [8] S. Ji, Y. Xue, and L. Carin, "Bayesian compressive sensing," *IEEE Trans. on Signal Proc.*, vol. 56, pp. 2346–2356, June 2008.
- [9] S. D. Babacan, R. Molina, and A. K. Kataaggelos, "Bayesian compressive sensing using laplace priors," *IEEE Trans. Image. Pro.*, vol. 19, pp. 53–63, 2009.
- [10] D. Baron, S. Sarvotham, and R. G. Baraniuk, "Bayesian compressive sensing via belief propagation," *IEEE Trans. Signal. Pro.*, vol. 58, pp. 269–280, 2010.
- [11] M. F. Duarte, M. B. Wakin, and R. G. Baraniuk, "Wavelet-domain compressive signal reconstruction using a hidden markov tree model," in *IEEE Int. Conf. on Acoustics, Speech and Signal Processing (ICASSP)*, 2008, pp. 5137–5140.
- [12] V. Cevher, M. F. Duarte, C. Hegde, and R. G. Baraniuk, "Sparse signal recovery using markov random fields," in *Neural Information Processing System (NIPS)*, 2008.
- [13] S. Som and P. Schniter, "Compressive imaging using approximate message passing and a markov-tree prior," *IEEE Trans. Signal Processing*, vol. 60, no. 7, pp. 3439–3449, 2012.
- [14] L. He and L. Carin, "Exploiting structure in wavelet based bayesian compressive sensing," *IEEE Trans. on signal Proc.*, vol. 92, pp. 3488–3497, 2009.
- [15] L. Yu, C. Wei, and G. Zheng, "Adaptive bayesian estimation with cluster structured sparsity," *Signal Proc. Letters*, vol. 22, pp. 2309–2313, 2015.
- [16] Y. Kim, M. S. Nadar, and A. Bilgin, "Wavelet-based compressed sensing using a gaussian scale mixture model," *IEEE Trans. Image Process.*, vol. 21, no. 6, pp. 3102–3110, June 2012.
- [17] J. P. Vila and P. Schniter, "Expectation-maximization gaussian-mixture approximate message passing," *IEEE Trans. Signal Process.*, vol. 61, pp. 4685–4672, October 2013.
- [18] Y. Ma, J. Zhu, and D. Baron, "Approximate message passing algorithm with universal denoising and gaussian mixture learning," *IEEE Trans. on signal processing*, vol. 64, no. 21, pp. 5611–5622, November 2016.
- [19] X. Lan and K. E. Barner, "Field of experts: Optimal structured bayesian compressed sensing," in *IEEE Global Conf. on Signal and Information Proc.*, 2017, pp. 1130–1134.
- [20] J. Portilla, V. Strela, M. J. Wainwright, and E. P. Simoncelli, "Image denoising using scale mixtures of gaussians in the wavelet domain," *IEEE Trans. on Image Proc.*, pp. 1338–1351, 2003.
- [21] G. Hinton, L. Deng, D. Yu, G. Dahl, A. Mohamed, N. Jaitly, A. Senior, V. Vanhoucke, P. Nguyen, T. Sainath, and B. Kingsbury, "Deep neural networks for acoustic modeling in speech recognition," *IEEE Signal Processing Magazine*, 2012.
- [22] Krizhevsky, S. A., and G. E. Hinton, "Imagenet classification with deep convolutional neural networks," in *NIPS*, vol. 25, 2012, pp. 1090–1098.
- [23] Y. Bengio, A. Courville, and P. Vincent, "Representation learning: A review and new perspectives," *IEEE Trans. on Pattern Analysis and Machine Intelligence*, vol. 35, no. 8, pp. 1798–1828, Aug. 2013.
- [24] D. E. Rumelhart, G. E. Hinton, and R. J. Williams, "Learning representations by back-propagating errors," *Nature*, vol. 323, pp. 533–536, October 1986.
- [25] K. Kulkarni, S. Lohit, P. Turaga, R. Kerchiche, and A. Ashok, "Reconnet: Non-iterative reconstruction of images from compressively sensed measurements," in *IEEE Conf. on CVPR*, June 2016.
- [26] H. Yao, F. Dai, D. Zhang, Y. Ma, S. Zhang, and Y. Zhang, "Dr2-net: Deep residual reconstruction network for image compressive sensing," *arXiv preprint arXiv:1702.05743*, 2017.

- [27] K. H. Jin, M. T. McCann, E. Froustey, and M. Unser, "Deep convolutional neural network for inverse problems in imaging," *IEEE Trans. on Image Process.*, vol. 9, no. 26, pp. 4509–4522, 2017.
- [28] A. Mousavi and R. G. Baraniuk, "Learning to invert: Signal recovery via deep convolutional networks," in *IEEE International Conference on Acoustics, Speech and Signal Processing (ICASSP)*, 2017.
- [29] C. A. Metzler, A. Mousavi, and R. G. Baraniuk, "Learned d-amp: principled neural network based compressive image recovery," *arXiv preprint arXiv:1704.06625*, 2017.
- [30] A. Nguyen, J. Yosinski, and J. Clune, "Deep neural networks are easily fooled: High confidence predictions for unrecognizable images," in *IEEE Conf. on CVPR*, July 2015, pp. 427–436.
- [31] M. Seyed, D. Moosavi, F. Alhussein, and F. Pascal, "Deepfool: A simple and accurate method to fool deep neural networks," in *IEEE Conf. on CVPR*, June 2017, pp. 2574–2582.
- [32] N. Carlini and D. Wagner, "Towards evaluating the robustness of neural networks," in *IEEE Symposium on Security and Privacy*, May 2017.
- [33] G. Alain and Y. Bengio, "Understanding intermediate layers using linear classifier probes," *arXiv preprint arXiv:1610.01644*, 2016.
- [34] S. Geman and D. Geman, "Stochastic relaxation, gibbs distributions, and the bayesian restoration of images," *IEEE Trans. on Pattern Analysis and Machine Intelligence*, pp. 721–741, June 1984.
- [35] S. Z. Li, *Markov Random Field Modeling in Image Analysis 2nd ed.* New York: Springer-Verlag, 2001.
- [36] S. Zhu and D. Mumford, "Prior learning and gibbs reaction-diffusion," *IEEE Trans. on Pattern Analysis and Machine Intelligence*, vol. 19, pp. 1236–1250, November 1997.
- [37] H. Boullard and C. Wellekens, "Links between markov models and multilayer perceptrons," in *NIPS*, 1989, pp. 502–510.
- [38] Z. Wu, D. Lin, and X. Tang, "Deep markov random field for image modeling," in *European Conference on Computer Vision (ECCV)*, 2016, pp. 295–312.
- [39] J. Bridle, "Training stochastic model recognition algorithms as networks can lead to maximum mutual information estimation of parameters," in *In Advances in Neural Information Processing Systems (NIPS)*, 1990.
- [40] Y. LeCun, S. Chopra, R. Hadsell, M. Ranzato, and F. Huang, *A tutorial on energy-based learning*. MIT Press: Predicting Structured Data, 2006.
- [41] S. Zheng, S. Jayasumana, B. Romera-Paredes, V. Vineet, Z. Su, D. Du, C. Huang, and P. Torr, "Conditional random fields as recurrent neural networks," in *International Conference on Computer Vision (ICCV)*, 2015, pp. 1529–1537.
- [42] X. Lan and K. E. Barner, "From mrfs to cnns: A novel image restoration method," in *52nd Annual Conference on Information Sciences and Systems (CISS)*, 2018, pp. 1–5.
- [43] K. He, X. Zhang, S. Ren, and J. Sun, "Deep residual learning for image recognition," in *CVPR*, 2016, pp. 770–778.
- [44] T. Cover and J. Thomas, *Elements of Information Theory*. Hoboken, New Jersey: Wiley-Interscience, 2006.
- [45] N. Z. Naftali Tishby, "Deep learning and the information bottleneck principle," *arXiv preprint arXiv:1503.02406*, 2015.
- [46] R. Shwartz-Ziv and N. Tishby, "Opening the black box of deep neural networks via information," *arXiv preprint arXiv:1703.00810*, 2017.
- [47] I. Goodfellow, J. Shlens, and C. Szegedy, "Explaining and harnessing adversarial examples," *arXiv preprint arXiv:1412.6572*, 2014.
- [48] C. Xie, Y. Wu, L. V. Maaten, A. Yuille, and K. He, "Feature denoising for improving adversarial robustness," *arXiv preprint arXiv:1812.03411*, 2014.
- [49] C. Szegedy, W. Zaremba, I. Sutskever, J. Bruna, D. Erhan, I. Goodfellow, and R. Fergus, "Intriguing properties of neural networks," *arXiv preprint arXiv:1312.6199*, 2013.
- [50] G. E. Hinton, "Training products of experts by minimizing contrastive divergence," *Neural Computation*, vol. 14, pp. 1771–1800, 2002.
- [51] M. A. Carreira-Perpinan and G. E. Hinton, "On contrastive divergence learning," *Artificial Intelligence and Statistics*, pp. 33–41, 2005.
- [52] D. Geman and C. Yang, "Nonlinear image recovery with half-quadratic regularization," *IEEE Trans. Image Processing*, vol. 4, pp. 932–946, 1995.
- [53] M. J. Wainwright and E. P. Simoncelli, "Scale mixtures of gaussians and the statistics of natural images," in *NIPS*, 2000, pp. 855–861.
- [54] R. Tibshirani, "Regression shrinkage and selection via the lasso," *Journal of Royal Statistical Society. Series B (Methodological)*, vol. 58, pp. 267–288, 2006.
- [55] C. Li, "An efficient algorithm for total variation regularization with applications to the single pixel camera and compressive sensing," Master's thesis, Rice University, Houston, Texas, 2009.
- [56] D. Martin, C. Fowlkes, D. Tal, and J. Malik, "A database of human segmented natural images and its application to evaluating segmentation algorithms and measuring ecological statistics," in *Proc. 8th Int'l Conf. Computer Vision*, vol. 2, July 2001, pp. 416–423.



Xinjie Lan (S'17) received the B.S.E.E. degree from Yantai University, Shandong, China, in 2010. He received the M.S.E.E. degree from Beijing Institute of Technology, Beijing, China, in 2012. From 2012 to 2014, He was an Assistant Engineer with Beijing Institute of Telemetry Technology, Beijing, China. He is currently a PhD candidate with the Department of Electrical and Computer Engineering, University of Delaware. His research interests include statistical signal processing, deep learning, inverse problem, compressed sensing, and image restoration.



Kenneth E. Barner (S'84-M'92-SM'00-F'16) received the B.S.E.E. degree from Lehigh University, Bethlehem, Pennsylvania, in 1987. He received the M.S.E.E. and Ph.D. degrees from the University of Delaware, Newark, Delaware, in 1989 and 1992, respectively. He was the duPont Teaching Fellow and Visiting Lecturer with the University of Delaware in 1991 and 1992, respectively. From 1993 to 1997, he was an Assistant Research Professor with the Department of Electrical and Computer Engineering, University of Delaware, and a Research Engineer with the duPont Hospital for Children. He is currently Charles B. Evans Professor and Chairman with the Department of Electrical and Computer Engineering, University of Delaware.

His research interests include signal and image processing, robust signal processing, nonlinear systems, sensor networks and consensus systems, compressive sensing, human-computer interaction. Dr. Barner is the recipient of a 1999 NSF CAREER award. He was the Co-Chair of the 2001 IEEE-EURASIP Nonlinear Signal and Image Processing (NSIP) Workshop and a Guest Editor for a Special Issue of the EURASIP Journal of Applied Signal Processing on Nonlinear Signal and Image Processing. He was a member of the Nonlinear Signal and Image Processing Board. He was the Technical Program Co-Chair for ICASSP 2005 and previously served on the IEEE Signal Processing Theory and Methods (SPTM) Technical Committee and the IEEE Bio-Imaging and Signal Processing (BISP) Technical Committee. He is currently a member of the IEEE Delaware Bay Section Executive Committee. He has served as an Associate Editor of the IEEE Transactions on Signal Processing, the IEEE Transaction on Neural Systems and Rehabilitation Engineering, the IEEE Signal Processing Magazine, the IEEE Signal Processing Letters, and the EURASIP Journal of Applied Signal Processing. He was the Founding Editor-in-Chief of the journal Advances in Human-Computer Interaction.